The University of Southern Mississippi
The Aquila Digital Community

8-31-2018

Rational Design of Superhydrophilic/Superoleophobic Surfaces for Oil-Water Separation via Thiol-Acrylate Photopolymerization

Li Xiong
University of Southern Mississippi, li.xiong@usm.edu

Wei Guo
University of Southern Mississippi, wei.guo@usm.edu

Benjamin M. Alameda
University of Southern Mississippi

Reese Sloan
University of Southern Mississippi

William D. Walker
University of Southern Mississippi

See next page for additional authors

Follow this and additional works at: https://aquila.usm.edu/fac_pubs

Part of the Chemistry Commons

### Recommended Citation

Authors

Li Xiong, Wei Guo, Benjamin M. Alameda, Reese Sloan, William D. Walker, and Derek L. Patton

Rational Design of Superhydrophilic/Superoleophobic Surfaces for Oil–Water Separation via Thiol–Acrylate Photopolymerization

Li Xiong, Wei Guo, Benjamin M. Alameda, Reese K. Sloan, William D. Walker, and Derek L. Patton*

School of Polymer Science and Engineering, University of Southern Mississippi, Hattiesburg, Mississippi 39406, United States

ABSTRACT: We report a simple, rapid, and scalable strategy to fabricate surfaces exhibiting in-air superoleophobic/super-hydrophilic wetting via sequential spray deposition and photopolymerization of nanoparticle-laden thiol–acrylate resins comprising both hydrophilic and oleophobic chemical constituents. The combination of spray deposition with nanoparticles provides hierarchical surface morphologies with both micro- and nanoscale roughness. Mapping the wetting behavior as a function of resin composition using high- and low-surface-tension liquid probes enabled facile identification of coatings that exhibit a range of wetting behavior, including superhydrophilic/superoleophilic, super-hydrophobic/superoleophobic, and in-air superhydrophilic/ superoleophobic wetting. In-air superhydrophilic/superoleophobic wetting was realized by a dynamic rearrangement of the interface to expose a greater fraction of hydrophilic moieties in response to contact with water. We show that these in-air superoleophobic/superhydrophilic coatings deposited onto porous supports enable separation of model oil–water emulsions with separation efficiencies up to 99.9% with 699 L·m^{-2} h^{-1} permeate flux when the superhydrophilic/superoleophobic coatings are paired with 0.45 μm nylon membrane supports.
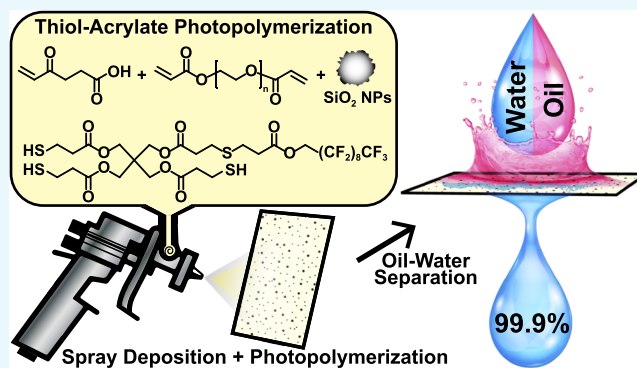
INTRODUCTION

Surface engineering strategies enabling the design of surfaces with special wetting properties—particularly superhydrophobic/superoleophilic and superhydrophilic/superoleophobic surfaces—have garnered significant attention for the oil–water separation processes for environmental cleanup, industrial wastewater treatment, and fuel decontamination.[1−5] Superhydrophobic/superoleophilic surfaces have been broadly explored as separation membranes that function on the premise of "oil removal"—a process requiring selective wetting of the surface by the low-surface-tension fluid to partition the oil and water phases.[6−13] However, oils readily foul these oleophilic surfaces, decreasing both flux and separation efficiency. Additionally, the higher density of water compared with most oils leads to a water barrier layer between the oil and the membrane, which hinders the separation process and often requires special engineering of the separation apparatus. In contrast, superhydrophilic/superoleophobic surfaces partition the oil and water phases based on the premise of "water removal", in which water selectively wets the surface and permeates through the membrane but oil is rejected. Such a design lowers the propensity of the surface being fouled by the oil phase and enables a gravity-driven separation process. Most separation membranes based on "water-removal" processes have relied on the design of superhydrophilic surfaces that exhibit underwater superoleophobicity and have been fabricated from a broad range of materials including zwitterionic polymers, hydrogels, and graphene oxide.[14−21] Superhydrophilic/underwater superoleophobic surfaces often

exhibit high oil–water separation efficiencies and low fouling; however, the design requires the membrane to be prewet with water prior to the separation process to avoid fouling.[22,23]

Surfaces exhibiting in-air superhydrophilicity and superoleophobicity are challenging to design—requiring an interface that simultaneously exhibits a surface energy higher than water and lower than oil. Thus, in practice, surfaces exhibiting both wetting properties simultaneously in air are rare, as super-oleophobic surfaces generally exhibit superhydrophobicity. The relatively few papers that have described the fabrication of superhydrophilic/in-air superoleophobic surfaces exploit a stimuli-responsive rearrangement of the material inter-face.[24−32] In 2012, Yang et al. reported a seminal approach to achieve superhydrophilic/superoleophobic wetting based on molecular rearrangement of interfaces comprising both hydro-philic and oleophobic chemical compositions.[25] Yang et al. reported the design of a superhydrophilic/superoleophobic nanocomposite film fabricated by spray-casting silica nano-particle/diallyldimethylammonium perfluorooctanoate solu-tions. Molecular rearrangement of the cationic and perfluoro groups at the interface enabled a transition from super-hydrophobic/superoleophobic to superhydrophilic/superoleo-phobic wetting behavior; however, the timescale for this transition was slow, requiring up to 9 min for the initial water contact angle (WCA) to decrease from 150° to 0°. The

transition timescale could be significantly decreased by plasma treating the surface, without extensively influencing the superoleophobicity. Similarly, Kota et al. reported hygroresponsive superhydrophilic/superoleophobic membranes based on cross-linked poly(ethylene glycol) containing fluorodecyl polyhedral oligomeric silsesquioxane (POSS).[24] Again, reorganization of the hydrophilic and oleophobic groups at the interface gave rise to superhydrophilic/superoleophobic membranes, where the timescale of the wetting transition was dependent on the concentration of POSS and the substrate type. For example, spin-coated silicon substrates and dip-coated wire-mesh substrates containing 20 wt % fluorodecyl POSS underwent surface reconfiguration in contact with water transitioning from a hydrophobic/superoleophobic state to a superhydrophilic/superoleophobic wetting state in less than 2.5 min, whereas coated textiles required up to 20 min for this transition. Kota employed these mesh membranes for separation of a range of oil–water mixtures with up to 99.9% separation efficiency without prewetting the membrane. Similarly, Pan and co-workers fluorinated the surface of cotton textiles with (tridecafluoro-1,1,2,2-tetrahydrooctyl)triethoxysilane to achieve superhydrophilic/superoleophobic wetting.[31] The superoleophobic wetting behavior was attributed to the fluorinated re-entrant morphology of the textile fibers, whereas superhydrophilicity was ascribed to reorganization of the cellulose chains in response to contact with polar liquids. These modified textiles were employed as efficient membranes for oil–water separations. Other approaches have included UV-light[33] and ammonia-triggered[28] transitions to achieve the superhydrophilic/superoleophobic wetting state. These examples illustrate simple strategies for the design of in-air superhydrophilic/superoleophobic surfaces based on synergistic interactions of interfacial chemistry, hierarchical roughness, and dynamic interfacial rearrangement. The details of other examples have been highlighted in several recent review articles.[2−4]

In a previous work, we demonstrated the fabrication of superhydrophobic[34] and superamphiphobic[35] coatings via spray deposition and photopolymerization of nanoparticle-laden thiol−ene resins. Herein, we describe a simple strategy to fabricate in-air superhydrophilic/superoleophobic surfaces by spray-coating nanoparticle-laden thiol−acrylate resins, resulting in hierarchically rough interfaces exhibiting both hydrophilic and oleophobic chemical constituents. Hydrophilic contributions at the material interface were achieved using 2-carboxyethyl acrylate, poly(ethyl glycol)diacrylate, and fumed silica nanoparticles, whereas oleophobic contributions were incorporated using a 1H,1H-perfluoro-n-decyl-modified multifunctional thiol. Composition versus wettability maps were used to identify surfaces with a range of wetting properties, including surfaces that display in-air superoleophobicity in contact with oil but rapidly transition (<10 s) to a superhydrophilic wetting state in contact with water via molecular rearrangement of the interface. A variety of porous substrates were coated with the superhydrophilic/superoleophobic resin and were employed for efficient separation of oil–water mixtures and oil–water emulsions.

■ RESULTS AND DISCUSSION

Resin Formulation, Film Fabrication, and Surface Morphology. Thiol−acrylate photopolymerization was employed to fabricate coatings exhibiting both superhydrophilic and superoleophobic wetting properties. As shown in Scheme 1, photopolymer resins were formulated with 2,2-dimethoxy-2-phenylacetophenone (DMPA) as a photoinitiator, poly-

Scheme 1. Spray-Deposition and Photopolymerization Process Using Hybrid Inorganic−Organic Thiol−Acrylate Resins Laden with Hydrophilic Silica Nanoparticles
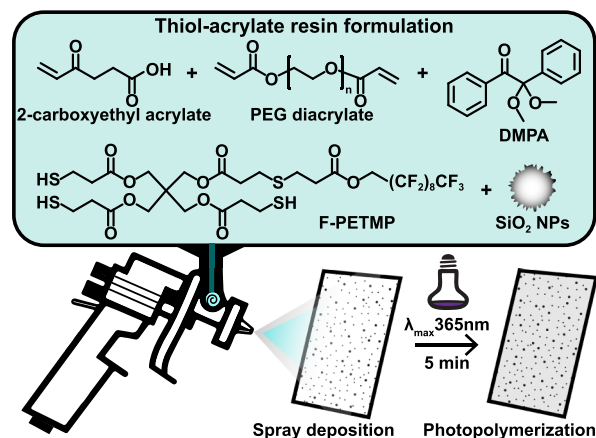
(ethylene glycol)diacrylate and 2-carboxyethyl acrylate as hydrophilic monomers (1:10 wt ratio), and 1H,1H-perfluoro-n-decyl-functionalized pentaerythritol tetra(3-mercaptopropionate) (F-PETMP) as an oleophobic resin constituent (20−50 wt % relative to the total acrylate resin). Thiol−acrylate photopolymerizations proceed via a dual-mode process involving simultaneous step-growth and chain-growth mechanisms.[36] Resins containing a 1:1 ratio of thiol to acrylate typically yield incomplete polymer networks with residual thiol functionality in the polymer matrix. Thus, to achieve high conversion of both acrylate and thiol functional groups, we explored resins formulated with excess acrylate. The molar ratios of the acrylate group to the thiol group were calculated as 13.7:1 (20 wt % F-PETMP), 8:1 (30 wt % F-PETMP), 6.8:1 (40 wt % F-PETMP), and 4.9:1 (50 wt % F-PETMP). Raman spectroscopy was used to investigate the photopolymerization behavior of the thiol−acrylate resins as a function of increasing the F-PETMP concentration. Figure 1a shows the series of Raman spectra for thiol−acrylate resins containing 20−50 wt % F-PETMP before exposure to UV light. The thiol (2569 cm^{-1}) and alkene (1634 cm^{-1}) peaks are highlighted in yellow and blue, respectively. Figure 1b shows the Raman spectra of the thiol−acrylate formulations after UV exposure. The acrylate group proceeded to high conversion in all the formulations as evidenced by the total disappearance of the characteristic peak at 1634 cm^{-1}. The thiol group, however, showed conversions that were dependent on the F-PETMP loading level. As shown in Figure 1c, thiol conversion decreased with increasing F-PETMP content because of the competing reactions of acrylate homopolymerization and thiol−acrylate step-growth polymerization. At 20 and 30 wt % F-PETMP loading levels, thiol conversion was ∼96.6%, which indicates that the thiol functional groups were mostly consumed in the step-growth process. When F-PETMP was increased to 50 wt %, the conversion of thiol decreased to ∼83.6%, indicative of the competitive chain-growth and step-growth processes. The polymerization behavior observed herein is consistent with other reports involving thiol−acrylate photopolymerizations.[37,38]
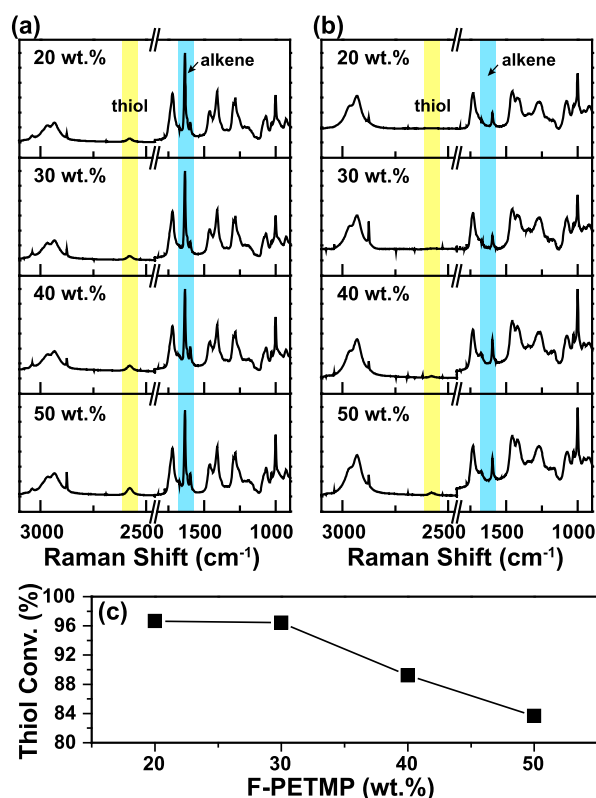
Figure 1. Raman spectra for the thiol–acrylate films with different F-PETMP contents (a) before and (b) after UV exposure. (c) Calculated thiol conversion as a function of F-PETMP concentration.

Figure 2. SEM micrographs of F-PETMP(30)/SiO$_2$(50) at (a) low and (b) high magnification; (c) EDS spectrum of F-PETMP(30)/SiO$_2$(50) and elemental map of control, F, S, and Si, respectively.

Element	C	O	F	Si	S	Ag	Total
Wt %	24.8	34.16	8.78	22.78	3.8	5.68	100

Next, fumed silica nanoparticles were added into the resin at various loading levels (30−60 wt % relative to the resin). To simplify the notation for each system, we will represent the various formulations as F-PETMP(x)/SiO$_2$(y), where x and y represent the weight percentage of F-PETMP and SiO$_2$, respectively. The resins were formulated by diluting the constituents with acetone and homogenizing the mixture with ultrasonication. The resins were then spray-coated onto various substrates (e.g., glass, wire-mesh, cotton-textile, and nylon membranes) using a simple airbrush device and cured under UV light as previously reported.[34,35] The spray-deposition method provides a simple route to endow the thiol−acrylate coating with the hierarchical roughness necessary to achieve the desired superhydrophilic, super-hydrophobic, and superoleophobic wetting behavior. The surface morphology of the spray-coated and photocured thiol−acrylate films was investigated using scanning electron microscopy (SEM). Figure 2a shows the SEM image of the F-PETMP(30)/SiO$_2$(50) sample at a low magnification. The surface exhibits a similar morphology to our earlier work, with randomly distributed micrometer and sub-micrometer agglomerations that can be attributed to the spray-deposition process. The higher magnification image (Figure 2b) clearly shows that the micrometer scale aggregates are superimposed with a nanometer-scale roughness that arises from the fumed silica aggregates. The combination of micro- and sub-micrometer-sized particles endows the surface with a porous, hierarchically structured morphology. Energy-dispersive spectroscopy (EDS) analysis was used to explore the elemental surface composition of the F-PETMP(30)/SiO$_2$(50) sample. As shown in Figure 2c, the surface was primarily composed of F, S, Si, C, and O
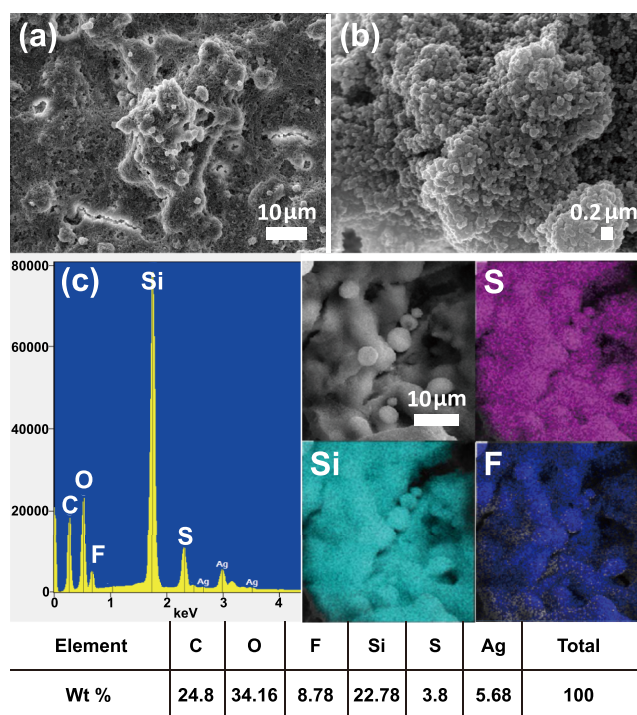
elements. The presence of sulfur and silicon in the EDS originates from the trifunctional thiol and fumed silica nanoparticles, respectively. The fluorine content of the cured film obtained from EDS was 8.78 ± 0.13 wt %, whereas the fluorine content calculated from the bulk resin composition for F-PETMP(30)/SiO$_2$(50) was 5.33 wt %. The higher F content observed by EDS is indicative of surface enrichment of the low-surface-energy F-PETMP component, and is consistent with previous observations using X-ray photoelectron spectroscopy.[35] Further, the EDS elemental mapping of F, S, and Si indicated that all elements were well distributed across the surface of the coating.

Wetting Behavior. The wetting properties of the films were evaluated via contact angle measurements. Hexadecane (γ = 27 mN/m) and deionized water (γ = 72.4 mN/m) were used as the probe liquids for oil contact angle (OCA) and WCA measurements, respectively. Figure 3a shows the wetting behavior of the nontextured (e.g., excluding silica nanoparticles from the formulation and spin-casting to smooth films on glass substrates) photocured films containing 0−50 wt % of F-PETMP. Here, it is necessary to mention that the WCA on many of these surfaces changed with time (as discussed below); thus, WCAs were consistently recorded 60 s after placing the droplet in contact with the surface. The OCAs did not show time-dependent behavior. As expected, the non-fluorinated film was completely wetted by both hexadecane (OCA = 4.6 ± 0.9°) and water (WCA = 8.6 ± 0.8°) because of the absence of a low-surface-energy component and the hydrophilic nature of the acidic acrylate resin. Incorporation of 20 wt % F-PETMP resulted in films with hydrophilic WCA (24.6 ± 0.6°), indicating a strong contribution from the polar carboxylic acid groups in the resin. Further increasing the concentration of F-PETMP resulted in transition from hydrophilic to hydrophobic wetting behavior, with the WCA
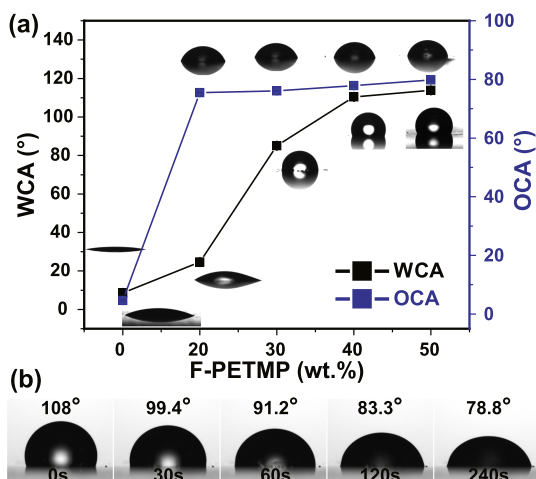
Figure 3. (a) WCA (black line) and OCA (blue line) change with the variation of F-PETMP content of nontextured films. The inserted images are representative photographs of water and oil droplets (6 μL) on the nontextured surfaces. (b) Time-dependent wetting of water on the F-PETMP(30) surface.

increasing from 85.1 ± 0.5° at 30 wt % F-PETMP to 113.8 ± 0.8° at 50 wt % F-PETMP. An example of the time-dependent wetting of water on the film containing 30 wt % F-PETMP is illustrated in Figure 3b. The time-dependent wetting arises from rearrangement of the carboxylic acid and fluorocarbon moieties at the contact interface; however, the time scale for the changes in the WCA is longer on the nontextured surface when compared to the hierarchically rough surfaces described below. In contrast, the OCA increased to 75.5 ± 0.7° with 20 wt % F-PETMP but showed only a small change in the OCA with further additions of F-PETMP (30−50 wt %) to the resin. This observation can be attributed to the saturation of the $1H,1H$-perfluoro-n-decyl-functional groups at the film surface—a result consistent with our previous work with F-PETMP.[35]

With insights into the wetting properties of nontextured films, we next investigated the wetting behavior of the same resin compositions containing silica nanoparticles deposited onto glass substrates via spray deposition, where the hierarchical roughness of the surface is expected to significantly influence the wetting and antiwetting characteristics of the surface. In these experiments, the SiO_2 nanoparticle content was varied from 30 to 60 wt % relative to the total weight of the resin, whereas the F-PETMP concentration was varied from 20 to 50 wt % relative to the acrylate. Figure 4a,b shows the WCA and OCA, respectively, as a function of the SiO_2 nanoparticle and the F-PETMP loading levels. Specific values for the contact and sliding angles are given in Table 1. From the detailed wetting/composition maps in Figure 4, the compositions can be identified to design surfaces that balance the contributions from the high-surface-energy carboxylic acid and silanol functional groups with contributions from the low-surface-energy fluorocarbon groups to achieve a range of desired wetting behavior. For example, the films fabricated without F-PETMP exhibited low contact angles (<5°) for both water and oil as the SiO_2 content changed from 30 to 60 wt %—observations that are associated with superhydrophilic and superoleophilic wetting behavior. The superhydrophilic/superoleophilic wetting behavior is demonstrated in Figure 4c, where vegetable oil, hexadecane, and water are observed to
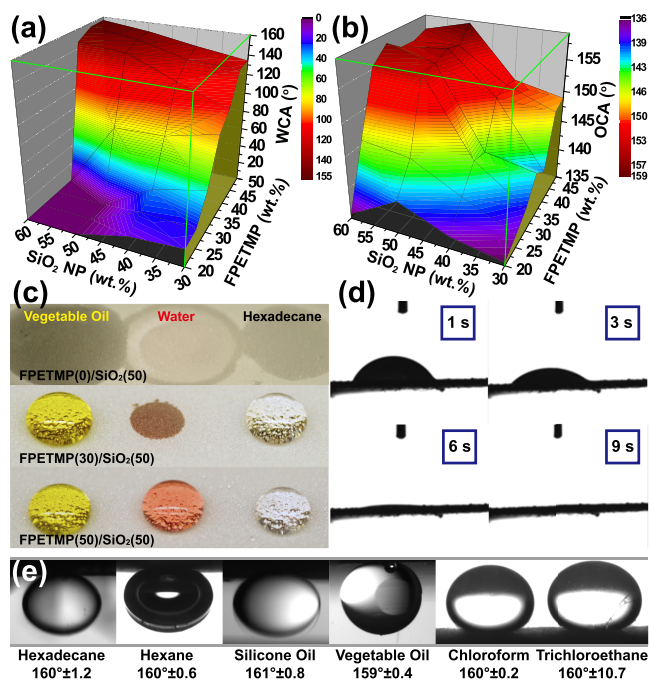

Figure 4. Variation of (a) WCA and (b) OCA as a function of SiO_2 nanoparticle and F-PETMP loading level. (c) Photo of vegetable oil, water, and hexadecane droplets on the surface of samples F-PETMP(0)SiO$_2$(50), F-PETMP(30)SiO$_2$(50), and F-PETMP(50)-SiO$_2$(50). (d) Time-dependent decrease in contact angle for a water droplet on the F-PETMP(30)SiO$_2$(50) surface on a 0.45 μm nylon membrane support. (e) Photos and contact angles of underwater oil droplets in contact with the F-PETMP(30)SiO$_2$(50) surface.

Table 1. Wetting Properties for Sprayed F-PETMP/SiO$_2$ Thiol−Acrylate Thin Films

SiO$_2$ (%) (y)	WCA (deg)	WSA (deg)	OCA (deg)	OSA (deg)
	F-PETMP(20)/SiO$_2$(y)			
30	18.7 ± 0.4		135.5 ± 1.6	
40	14.5 ± 0.8		136.9 ± 1.9	
50	0		140.1 ± 2.0	
60	0		135.7 ± 1.1	
	F-PETMP(30)/SiO$_2$(y)			
30	45.7 ± 1.1		138.7 ± 1.7	
40	32.1 ± 0.5		144.2 ± 2.1	
50	0		155.6 ± 1.0	10 ± 1
60	0		155.3 ± 0.9	12 ± 1
	F-PETMP(40)/SiO$_2$(y)			
30	103.6 ± 0.7		140.2 ± 0.6	
40	121.9 ± 1.1		150.5 ± 1.5	
50	142.8 ± 0.9		156.1 ± 0.9	7 ± 2
60	146.7 ± 1.3		155.9 ± 0.8	7 ± 1
	F-PETMP(50)/SiO$_2$(y)			
30	134.3 ± 0.6		148.9 ± 1.4	
40	141.8 ± 1.2		150.5 ± 0.7	12 ± 2
50	150.6 ± 0.8	5 ± 1	158.6 ± 0.8	7 ± 1
60	156.6 ± 0.9	5 ± 1	156.7 ± 1.0	8 ± 1

completely wet the F-PETMP(0)/SiO$_2$(50) surface. At the other extreme in composition, the films containing 40−50 wt % F-PETMP exhibited WCA−OCAs ranging from 104°/140° when loaded with 30 wt % SiO_2 to 156°/157° when loaded with 60 wt % SiO_2—characteristic behavior that approaches superhydrophobic and superoleophobic wetting, as demon-
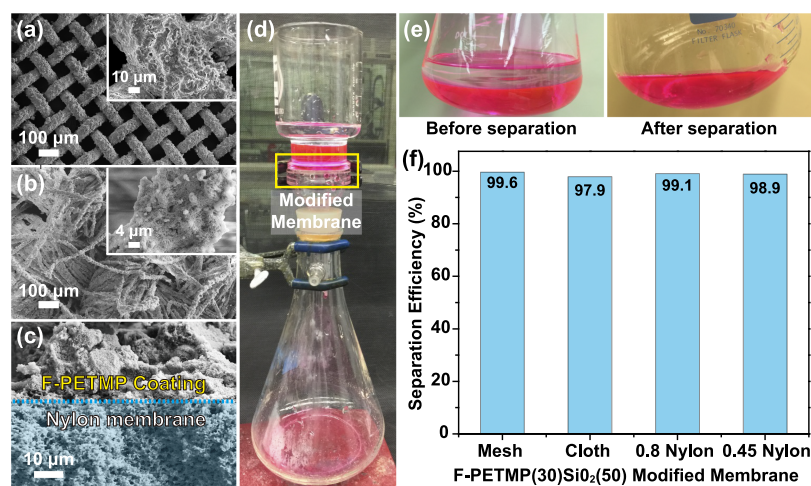
Figure 5. SEM micrographs of F-PETMP(30)/SiO$_2$(50) spray-coated onto (a) a stainless-steel mesh, (b) a cotton-textile, and (c) a 0.45 μm nylon membrane (the nylon membrane was colored blue in the cross section image for clarity). (d) Photographs of the simple, gravity-driven apparatus employed for oil–water separation. (f) Separation efficiency for surfactant-free oil–water mixtures.

strated in Figure 4c. Notably, the F-PETMP(30)/SiO$_2$(50) surface exhibited a WCA of 0°, an OCA of 155.6 ± 1°, and a 10 ± 1° oil sliding angle (OSA) indicative of the desired superhydrophilic and superoleophobic wetting behavior. The in-air superhydrophilic/superoleophobic wetting behavior of the F-PETMP(30)/SiO$_2$(50) film is illustrated in Figure 4c, where vegetable oil and hexadecane interact with the surface with OCAs greater than 150°, whereas water completely wets the surface. We postulate that the composition of the F-PETMP(30)/SiO$_2$(50) film strikes an appropriate balance between carboxylic acid and fluorocarbon moieties, enabling a dynamic rearrangement of the interface to expose a greater fraction of COOH groups in response to contact with water; rearrangement results in a fully wetted interface. Similarly, fluorocarbon moieties are preferentially presented at the interface in response to contact with a low-surface-tension liquid, resulting in a nonwetted interface. As reported by others, the rearrangement of the interface is not instantaneous.[24,25,39] The dynamic nature of the wetting process with water can be observed as a function of time. As illustrated in Figure 4d, a water droplet initially interacts with the F-PETMP(30)/SiO$_2$(50) surface with a finite contact angle (57.2 ± 1°), but transitions rapidly (<10 s) to a fully wetted state with a 0° contact angle. This transition time is relatively fast in comparison to that of some materials reported in the literature, particularly considering that no additional processing steps were required.[24,25] However, it is important to note that the transition time appears to be highly dependent on multiple parameters (composition, crystallinity, substrate, etc.), making direct comparisons across the literature difficult.

Lastly, based on the observed in-air wetting behavior of the F-PETMP(30)/SiO$_2$(50) surface, we can expect these surfaces to also exhibit underwater superoleophobicity. Thus, the underwater oil-wetting behavior of the F-PETMP(30)/SiO$_2$(50) film was examined. Contact angle measurements were obtained underwater using a series of low-surface-tension liquids, including hexadecane, hexane, silicone oil, vegetable oil, chloroform, and trichloroethane. As shown in Figure 4e, the spray-coated F-PETMP(30)/SiO$_2$(50) film exhibited underwater OCAs larger than 150° for each oil, confirming an underwater superoleophobic wetting behavior. Furthermore, these oil droplets showed low sliding angles (<1°) in the

underwater environment, indicating minimal adhesion between the oil droplets and the surface.

Oil–Water Separation. The superhydrophilic/superoleophobic F-PETMP(30)/SiO$_2$(50) resin was selected for the fabrication of oil–water separation membranes. The F-PETMP(30)/SiO$_2$(50) coatings were fabricated via spray deposition on a series of substrates serving as supports for the composite separation membrane, including stainless-steel mesh (200 mesh size), cotton cloth, and nylon filters (0.8 and 0.45 μm pore size). SEM images of the F-PETMP(30)/SiO$_2$(50) coating on the various supports are shown in Figure 5a–c. The spray-deposition process provided conformal, hierarchically rough coatings on the strands of the stainless-steel mesh (Figure 5a) and the fibers comprising the cotton textile (Figure 5b) without blocking the inherent microporosity of these substrates. Similarly, the process yields a conformal F-PETMP(30)/SiO$_2$(50) coating on the 0.45 μm nylon membrane, as shown in the cross-sectional image in Figure 5c. Initially, we evaluated the composite membranes for the separation of surfactant-free hexane and water mixtures. Figure 5d shows the simple apparatus, consisting of the composite membranes sandwiched between the upper and lower pieces of a glass filtration device, employed for gravity-driven separations. The water layer was dyed pink with sulforhodamine B to improve the visibility of the separation process. The hexane–water mixtures were mechanically agitated and then poured into a glass funnel. Because of the in-air superoleophobicity and rapid transition to a superhydrophilic wetting state upon contact with water, prewetting the membrane with water was unnecessary. As shown, water passed through the membrane driven by gravity, whereas hexane was rejected by the membrane and remained in the separation funnel. The calculated separation efficiencies, shown in Figure 5f, were greater than 98% for each composite membrane investigated.

Oil-in-water emulsions are more commonly encountered in the treatment of industrial wastewater and in environmental cleanup scenarios, where a surfactant typically results in the oil being dispersed as small droplets within the aqueous phase.[40] For separation of emulsions, we focused attention on F-PETMP(30)/SiO$_2$(50) coatings supported by the nylon membrane with 0.45 and 0.8 μm pore sizes. A hexadecane-

in-water emulsion stabilized using sodium dodecyl sulfate (SDS) as the surfactant (hydrophilic–lipophilic balance = 40) was employed as a model feed. The same separation apparatus was used as previously described, except that a negative pressure (−30 kPa) was applied to the collection flask. Figure 6a shows photographs of the hexadecane-in-water emulsion
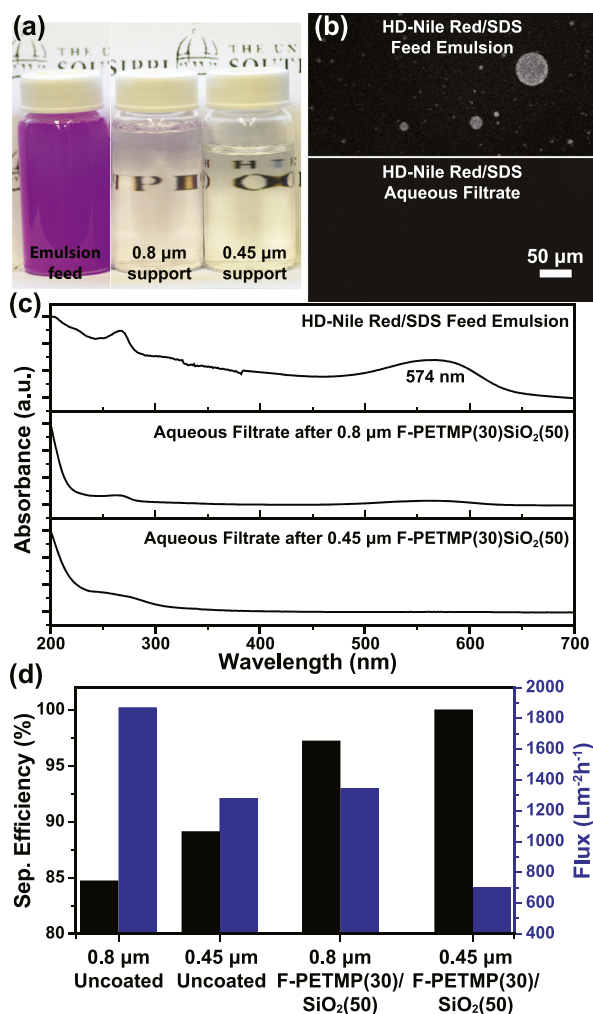

Figure 6. Photos of (a) hexadecane-in-water emulsion feeds before and after separation using the F-PETMP(30)/SiO$_2$(50)-coated nylon membranes. (b) Confocal microscope images of the hexadecane-in-water emulsion feed and water collected after separation with the F-PETMP(30)/SiO$_2$(50) 0.45 μm nylon membrane. (c) UV–vis spectra of the hexadecane-in-water/Nile red emulsion before separation and after separation with nylon membranes coated with F-PETMP(30)/SiO$_2$(50). (d) Separation efficiency and flux vs nylon support pore size for hexadecane-in-water/Nile red emulsions.

feed before and after separation using the F-PETMP(30)/SiO$_2$(50)-coated membranes. Before separation, emulsions consisted of droplets ranging in size from hundreds of nanometers to tens of micrometers, as exemplified by confocal imaging of the hexadecane/Nile red feed in Figure 6b. After separation, the presence of droplets in the collected filtrate was difficult to discern by confocal microscopy. To determine the separation efficiency, the concentration of hexadecane in water was determined using UV–vis spectroscopy (λ = 574 nm for Nile red/hexadecane), as shown in Figure 6c. The separation efficiencies and flux values are shown in Figure 6d. The

separation efficiencies for the uncoated 0.8 and 0.45 μm nylon supports were 84.7 and 89.1%, respectively. In general, decreasing the pore size of the membrane support resulted in an improved separation efficiency; however, the flux decreased from 1868 L·m^{-2} h^{-1} for the 0.8 μm membrane to 1277 L·m^{-2} h^{-1} for the 0.45 μm membrane. Although separation of the hexadecane-in-water emulsion could be achieved using the uncoated membranes, these membranes were readily fouled by the oil-in-water emulsion. As shown, coating the nylon supports with the F-PETMP(30)/SiO$_2$(50) coating improved the separation efficiencies. The F-PETMP(30)/SiO$_2$(50) coating on the 0.45 μm nylon substrate provided the best separation performance, yielding a 99.9% efficiency for the hexadecane-in-water emulsion. However, the increase in separation efficiency is achieved at the expense of the permeate flux. For example, the flux decreased from 1343 L·m^{-2} h^{-1} for separation of the hexadecane-in-water on the 0.8 μm nylon support to 699 L·m^{-2} h^{-1} when using the 0.45 μm nylon support. These separation efficiencies and flux values are comparable to the performance of a broad range of separation membranes reported in the literature.[1]

CONCLUSIONS

In this paper, we have demonstrated a quick and simple approach to fabricate superhydrophilic/superoleophobic coatings via spray deposition and UV photopolymerization of perfluorinated thiol/acidic acrylate resins containing hydrophilic silica nanoparticles. The spray-deposition method of the nanoparticle-laden resins provided coatings with hierarchically rough morphologies on a broad range of substrates. Resin composition versus wettability mapping using high- and low-surface-tension liquid probes enabled facile identification of coatings that exhibit a range of wetting behavior, including superhydrophilicity/superoleophilicity, superhydrophobicity/superoleophobicity, and in-air superhydrophilicity/superoleophobicity. The superhydrophilic/superoleophobic coatings were evaluated as membranes for separation of oil-in-water mixtures and oil-in-water emulsions. Separation efficiencies up to 99.9% with 699 L·m^{-2} h^{-1} permeate flux were achieved when the superhydrophilic/superoleophobic coatings were paired with 0.45 μm nylon membrane supports. A salient feature of the fabrication process is scalability to large-area substrates. We anticipate that simplicity and scalability of the fabrication process and the efficiency of oil–water separations will lead to broad applications of these membranes for the treatment of oil spills and industrial wastewater streams.

EXPERIMENTAL SECTION

Materials. All reagents were obtained at the highest purity available and used without further purification unless otherwise specified. 2-Carboxyethyl acrylate, poly(ethyl glycol)diacrylate 400, DMPA, and acetone were obtained from Sigma-Aldrich, PETMP was obtained from Bruno Bock. F-PETMP was synthesized according to the literature.[41] Aerosil R380, hydrophilic fumed silica with a hydroxyl surface and an average primary particle size of 16 nm was kindly provided by Evonik Industries.

Characterization. Contact angle measurements were performed using a Rame-Hart 200-00 Std.-Tilting B. goniometer. Static contact angles were measured using 6 μL water droplets. ImageJ Drop Analysis was used to analyze the droplets. SEM images were obtained using a Zeiss Sigma VP

FEG-SEM at 10 kV in high-vacuum mode. Raman spectroscopy was conducted using an iRaman Plus. The thiol conversion was monitored by measuring the area of the thiol absorption peak at 2576 cm^{-1}. Conversions were calculated with the ratio of the peak area to the peak area prior to polymerization. All reactions were performed under ambient conditions. Transmission electron micrographs (TEMs) (Digital Imaging with Gatan model 785 ES1000W Erlangshen CCD Camera) were taken with a Zeiss 900 TEM operating at 50 kV. UV−vis spectra were obtained by using a PerkinElmer Lambda 35 UV−vis spectrometer. Optical microscope images were obtained by using an Olympus BX52 digital optical microscope system. Dynamic light scattering analysis was conducted using a Microtrac Nanotrac Ultra. Confocal images were obtained using a Zeiss LSM 510 confocal laser-scanning microscope with a 543 nm HeNe laser.

Film Preparation. Thiol−acrylate-based hybrid resins were prepared by weighing out a trifunctional thiol (F-PETMP), hydrophilic alkene (2-carboxyethyl acrylate), cross-linker poly(ethyl glycol)diacrylate 400, and DMPA (5 wt %) into a glass jar. A specified amount of hydrophilic silica nanoparticles (SiO$_2$, Aerosil R380 = 30, 40, 50, 60 wt % relative to the resin) was added to the resin mixture. For the formulations containing F-PETMP, the functional monomer (F-PETMP) was added at 0, 20, 30, 40, and 50 wt % relative to the total organic resin, which gave the stoichiometric ratio of alkene to thiol of 13.7:1, 8:1, 6.8:1, and 4.9:1 accordingly. The hybrid mixture was diluted in acetone (20:1 w/w solvent/resin) and then treated with bath ultrasonication (Fisher Scientific Ultrasonic Cleaner) for 30 min. An air brush with a nozzle diameter of 0.635 mm (Paasch H#3 obtained from McMaster Carr) was connected to a compressed nitrogen source (30 psi) and used to spray-coat the resin onto substrates at a distance of 15 cm and at a rate of 2 mL/min. Different substrates were sprayed, including glass slides, stainless-steel mesh with 200 mesh size, cotton cloth, and nylon filter membranes with either a 0.8 or a 0.45 μm pore size. The coating was allowed to sit for 1 min before curing under a UV flood lamp (16 mW/cm^2) for 5 min.

Preparation and Separation of Oil-in-Water Mixtures and Emulsions. A surfactant-free oil−water mixture was prepared by mechanically mixing a 1:1 volume ratio of hexane and water. The aqueous phase was dyed with sulforhodamine B to improve the visibility during the separation process. Thiol−acrylate coatings on the stainless-steel mesh, cotton-cloth, or nylon filters served as the composite separation membrane. A simple separation apparatus was employed consisting of the composite membrane sandwiched between the upper and lower pieces of a glass vacuum filtration device. Separations of the surfactant-free oil−water mixtures were gravity-driven. The separation efficiency (E) of the surfactant-free oil−water mixtures was calculated using the following equation: E % = W_p/W_o at 100%, where W_o and W_p represent the weight of the water phase before and after separation, respectively. Oil-in-water emulsions were prepared by ultra-sonicating a mixture of water (500 g), hexadecane (5 g), Nile red (10 mg), and SDS (1.2 g). Oil-in-water emulsions were separated with a negative pressure (−30 kPa) applied to the collection flask. The separation efficiency of oil-in-water emulsions was determined according to a literature method.[42] The oil rejection coefficient (R) was calculated using the following equation: R % = $(C_o − C_p)/C_o \times /100\%$, where C_o and C_p represent the oil concentration in the original oil-in-

water emulsion and the aqueous filtrate, respectively. The oil concentration was determined using UV−vis spectroscopy (λ = 574 nm for Nile red/hexadecane). The permeate flux was calculated according to the following equation: flux = $V/S \cdot t$, where V is the volume of water separated per unit of time, S is the active membrane area in contact with the oil-in-water emulsion, and t is time.

■ AUTHOR INFORMATION
Corresponding Author
*E-mail: derek.patton@usm.edu. Twitter: @dereklpatton (D.L.P.).
ORCID ⊙
Derek L. Patton: 0000-0002-8738-4750

Author Contributions
The paper was written through the contributions of all the authors. All the authors have given approval to the final version of the paper.

Notes
The authors declare no competing financial interest.

■ REFERENCES
(1) Ge, M.; Cao, C.; Huang, J.; Zhang, X.; Tang, Y.; Zhou, X.; Zhang, K.; Chen, Z.; Lai, Y. Rational design of materials interface at nanoscale towards intelligent oil-water separation. *Nanoscale Horiz.* **2018**, 3, 235−260.
(2) Ma, Q.; Cheng, H.; Fane, A. G.; Wang, R.; Zhang, H. Recent Development of Advanced Materials with Special Wettability for Selective Oil/Water Separation. *Small* **2016**, 12, 2186−2202.
(3) Xue, Z.; Cao, Y.; Liu, N.; Feng, L.; Jiang, L. Special wettable materials for oil/water separation. *J. Mater. Chem. A* **2014**, 2, 2445−2460.
(4) Yong, J.; Chen, F.; Yang, Q.; Huo, J.; Hou, X. Superoleophobic surfaces. *Chem. Soc. Rev.* **2017**, 46, 4168−4217.
(5) Wang, B.; Liang, W.; Guo, Z.; Liu, W. Biomimetic super-lyophobic and super-lyophilic materials applied for oil/water separation: a new strategy beyond nature. *Chem. Soc. Rev.* **2015**, 44, 336−361.
(6) Feng, L.; Zhang, Z.; Mai, Z.; Ma, Y.; Liu, B.; Jiang, L.; Zhu, D. A Super-Hydrophobic and Super-Oleophilic Coating Mesh Film for the Separation of Oil and Water. *Angew. Chem.* **2004**, 116, 2046−2048.
(7) Zhang, W.; Shi, Z.; Zhang, F.; Liu, X.; Jin, J.; Jiang, L. Superhydrophobic and Superoleophilic PVDF Membranes for Effective Separation of Water-in-Oil Emulsions with High Flux. *Adv. Mater.* **2013**, 25, 2071−2076.
(8) Crick, C. R.; Gibbins, J. A.; Parkin, I. P. Superhydrophobic polymer-coated copper-mesh; membranes for highly efficient oil-water separation. *J. Mater. Chem. A* **2013**, 1, 5943−5948.
(9) Chen, Q.; de Leon, A.; Advincula, R. C. Inorganic-Organic Thiol-ene Coated Mesh for Oil/Water Separation. *ACS Appl. Mater. Interfaces* **2015**, 7, 18566−18573.
(10) Liu, D.; Yu, Y.; Chen, X.; Zheng, Y. Selective separation of oil and water with special wettability mesh membranes. *RSC Adv.* **2017**, 7, 12908−12915.
(11) Zhang, W.; Shi, Z.; Zhang, F.; Liu, X.; Jin, J.; Jiang, L. Superhydrophobic and Superoleophilic PVDF Membranes for Effective Separation of Water-in-Oil Emulsions with High Flux. *Adv. Mater.* **2013**, 25, 2071−2076.

(12) Ji, D.; Xiao, C.; An, S.; Liu, H.; Chen, K.; Hao, J.; Zhang, T. Preparation of PSF/FEP mixed matrix membrane with super hydrophobic surface for efficient water-in-oil emulsion separation. *RSC Adv.* **2018**, *8*, 10097−10106.

(13) Peng, J.; Deng, J.; Quan, Y.; Yu, C.; Wang, H.; Gong, Y.; Liu, Y.; Deng, W. Superhydrophobic Melamine Sponge Coated with Striped Polydimethylsiloxane by Thiol-Ene Click Reaction for Efficient Oil/Water Separation. *ACS Omega* **2018**, *3*, 5222−5228.

(14) Liu, M.; Wang, S.; Wei, Z.; Song, Y.; Jiang, L. Bioinspired Design of a Superoleophobic and Low Adhesive Water/Solid Interface. *Adv. Mater.* **2009**, *21*, 665−669.

(15) Cheng, Q.; Li, M.; Zheng, Y.; Su, B.; Wang, S.; Jiang, L. Janus interface materials: superhydrophobic air/solid interface and super-oleophobic water/solid interface inspired by a lotus leaf. *Soft Matter* **2011**, *7*, 5948−5951.

(16) Liu, Q.; Patel, A. A.; Liu, L. Superhydrophilic and Underwater Superoleophobic Poly(sulfobetaine methacrylate)-Grafted Glass Fiber Filters for Oil-Water Separation. *ACS Appl. Mater. Interfaces* **2014**, *6*, 8996−9003.

(17) Zhang, W.; Zhu, Y.; Liu, X.; Wang, D.; Li, J.; Jiang, L.; Jin, J. Salt-Induced Fabrication of Superhydrophilic and Underwater Superoleophobic PAA-g-PVDF Membranes for Effective Separation of Oil-in-Water Emulsions. *Angew. Chem., Int. Ed.* **2014**, *53*, 856−860.

(18) Yuan, T.; Meng, J.; Hao, T.; Wang, Z.; Zhang, Y. A Scalable Method toward Superhydrophilic and Underwater Superoleophobic PVDF Membranes for Effective Oil/Water Emulsion Separation. *ACS Appl. Mater. Interfaces* **2015**, *7*, 14896−14904.

(19) Yong, J.; Chen, F.; Fang, Y.; Huo, J.; Yang, Q.; Zhang, J.; Bian, H.; Hou, X. Bioinspired Design of Underwater Superaerophobic and Superaerophilic Surfaces by Femtosecond Laser Ablation for Anti- or Capturing Bubbles. *ACS Appl. Mater. Interfaces* **2017**, *9*, 39863−39871.

(20) Li, H.; Liang, T.; Lai, X.; Su, X.; Zhang, L.; Zeng, X. Vapor-liquid interfacial reaction to fabricate superhydrophilic and under-water superoleophobic thiol-ene/silica hybrid decorated fabric for oil/water separation. *Appl. Surf. Sci.* **2018**, *427*, 92−101.

(21) Du, Y.; Li, Y.; Wu, T. A superhydrophilic and underwater superoleophobic chitosan-TiO2 composite membrane for fast oil-in-water emulsion separation. *RSC Adv.* **2017**, *7*, 41838−41846.

(22) Li, J.; Li, D.; Yang, Y.; Li, J.; Zha, F.; Lei, Z. A prewetting induced underwater superoleophobic or underoil (super) hydro-phobic waste potato residue-coated mesh for selective efficient oil/water separation. *Green Chem.* **2016**, *18*, 541−549.

(23) Li, J.; Yan, L.; Li, H.; Li, W.; Zha, F.; Lei, Z. Underwater superoleophobic palygorskite coated meshes for efficient oil/water separation. *J. Mater. Chem. A* **2015**, *3*, 14696−14702.

(24) Kota, A. K.; Kwon, G.; Choi, W.; Mabry, J. M.; Tuteja, A. Hygro-Responsive Membranes for Effective Oil-Water Separation. *Nat. Commun.* **2012**, *3*, 1025.

(25) Yang, J.; Zhang, Z.; Xu, X.; Zhu, X.; Men, X.; Zhou, X. Superhydrophilic-superoleophobic coatings. *J. Mater. Chem.* **2012**, *22*, 2834−2837.

(26) Yang, J.; Song, H.; Yan, X.; Tang, H.; Li, C. Superhydrophilic and superoleophobic chitosan-based nanocomposite coatings for oil/water separation. *Cellulose* **2014**, *21*, 1851−1857.

(27) Yang, J.; Yin, L.; Tang, H.; Song, H.; Gao, X.; Liang, K.; Li, C. Polyelectrolyte-fluorosurfactant complex-based meshes with super-hydrophilicity and superoleophobicity for oil/water separation. *Chem. Eng. J.* **2015**, *268*, 245−250.

(28) Xu, Z.; Zhao, Y.; Wang, H.; Wang, X.; Lin, T. A Superamphiphobic Coating with an Ammonia-Triggered Transition to Superhydrophilic and Superoleophobic for Oil-Water Separation. *Angew. Chem., Int. Ed. Engl.* **2015**, *54*, 4527−4530.

(29) Su, C.; Yang, H.; Song, S.; Lu, B.; Chen, R. A magnetic superhydrophilic/oleophobic sponge for continuous oil-water separa-tion. *Chem. Eng. J.* **2017**, *309*, 366−373.

(30) Brown, P. S.; Bhushan, B. Mechanically Durable, Super-oleophobic Coatings Prepared by Layer-by-Layer Technique for Anti-Smudge and Oil-Water Separation. *Sci. Rep.* **2015**, *5*, 8701.

(31) Pan, S.; Guo, R.; Xu, W. Durable superoleophobic fabric surfaces with counterintuitive superwettability for polar solvents. *AIChE J.* **2014**, *60*, 2752−2756.

(32) Brown, P. S.; Atkinson, O. D. L. A.; Badyal, J. P. S. Ultrafast Oleophobic-Hydrophilic Switching Surfaces for Antifogging, Self-Cleaning, and Oil-Water Separation. *ACS Appl. Mater. Interfaces* **2014**, *6*, 7504−7511.

(33) Tang, H.; Fu, Y.; Yang, C.; Zhu, D.; Yang, J. A UV-driven superhydrophilic/superoleophobic polyelectrolyte multilayer film on fabric and its application in oil/water separation. *RSC Adv.* **2016**, *6*, 91301−91307.

(34) Sparks, B. J.; Hoff, E. F. T.; Xiong, L.; Goetz, J. T.; Patton, D. L. Superhydrophobic Hybrid Inorganic-Organic Thiol-ene Surfaces Fabricated via Spray-Deposition and Photopolymerization. *ACS Appl. Mater. Interfaces* **2013**, *5*, 1811−1817.

(35) Xiong, L.; Kendrick, L. L.; Heusser, H.; Webb, J. C.; Sparks, B. J.; Goetz, J. T.; Guo, W.; Stafford, C. M.; Blanton, M. D.; Nazarenko, S.; Patton, D. L. Spray-Deposition and Photopolymerization of Organic-Inorganic Thiol-ene Resins for Fabrication of Super-amphiphobic Surfaces. *ACS Appl. Mater. Interfaces* **2014**, *6*, 10763−10774.

(36) Cramer, N. B.; Bowman, C. N. Kinetics of thiol-ene and thiol-acrylate photopolymerizations with real-time Fourier transform infrared. *J. Polym. Sci., Part A: Polym. Chem.* **2001**, *39*, 3311−3319.

(37) Cramer, N. B.; Bowman, C. N. Kinetics of thiol-ene and thiol-acrylate photopolymerizations with real-time fourier transform infrared. *J. Polym. Sci., Part A: Polym. Chem.* **2001**, *39*, 3311−3319.

(38) Hoyle, C. E.; Bowman, C. N. Thiol-Ene Click Chemistry. *Angew. Chem., Int. Ed.* **2010**, *49*, 1540−1573.

(39) Wang, Y.; Gong, X. Special oleophobic and hydrophilic surfaces: approaches, mechanisms, and applications. *J. Mater. Chem. A* **2017**, *5*, 3759−3773.

(40) Zhang, W.; Liu, N.; Cao, Y.; Lin, X.; Liu, Y.; Feng, L. Superwetting Porous Materials for Wastewater Treatment: from Immiscible Oil/Water Mixture to Emulsion Separation. *Adv. Mater. Interfaces* **2017**, *4*, 1600029.

(41) Shin, J.; Nazarenko, S.; Hoyle, C. E. Effects of Chemical Modification of Thiol−Ene Networks on Enthalpy Relaxation. *Macromolecules* **2009**, *42*, 6549−6557.

(42) Wang, G.; He, Y.; Wang, H.; Zhang, L.; Yu, Q.; Peng, S.; Wu, X.; Ren, T.; Zeng, Z.; Xue, Q. A cellulose sponge with robust superhydrophilicity and under-water superoleophobicity for highly effective oil/water separation. *Green Chem.* **2015**, *17*, 3093−3099.